11532 *Biochemistry* **2009,** *48,* 11532–11545
DOI: 10.1021/bi901475g

BIOCHEMISTRY
including biophysical chemistry & molecular biology
Article

A Transition Path Ensemble Study Reveals a Linchpin Role for Mg^{2+} during Rate-Limiting ADP Release from Protein Kinase A†

Ilja V. Khavrutskii,*[,‡,§,#] Barry Grant,[§,#] Susan S. Taylor,[‡,#,∥] and J. Andrew McCammon[‡,§,#,∥]

[‡]*Howard Hughes Medical Institute,* [§]*Center for Theoretical Biological Physics,* [#]*Department of Chemistry and Biochemistry, and* [∥]*Department of Pharmacology, University of California San Diego, La Jolla, California 92093-0365*

Received August 23, 2009; Revised Manuscript Received November 2, 2009

ABSTRACT: Protein kinases are key regulators of diverse signaling networks critical for growth and development. Protein kinase A (PKA) is an important kinase prototype that phosphorylates protein targets at Ser and Thr residues by converting ATP to ADP. Mg^{2+} ions play a crucial role in regulating phosphoryl transfer and can limit overall enzyme turnover by affecting ADP release. However, the mechanism by which Mg^{2+} participates in ADP release is poorly understood. Here we use a novel transition path ensemble technique, the harmonic Fourier beads method, to explore the atomic and energetic details of the Mg^{2+}-dependent ADP binding and release. Our studies demonstrate that adenine-driven ADP binding to PKA creates three ion-binding sites at the ADP/PKA interface that are absent otherwise. Two of these sites bind the previously characterized Mg^{2+} ions, whereas the third site binds a monovalent cation with high affinity. This third site can bind the P-3 residue of substrate proteins and may serve as a reporter of the active site occupation. Binding of Mg^{2+} ions restricts mobility of the Gly-rich loop that closes over the active site. We find that simultaneous release of ADP with Mg^{2+} ions from the active site is unfeasible. Thus, we conclude that Mg^{2+} ions act as a linchpin and that at least one ion must be removed prior to pyrophosphate-driven ADP release. The results of the present study enhance understanding of Mg^{2+}-dependent association of nucleotides with protein kinases.

Protein kinases are a large superfamily of phosphoryl transferases involved in the regulation of diverse cellular processes including transcription and replication of DNA, biosynthesis of neurotransmitters, metabolism of carbohydrates and lipids, organelle trafficking, muscle contraction, and cell differentiation (*1*−*7*). Because of these critical regulatory roles and because protein kinase defects are associated with many diseases, protein kinases are obvious targets for drug design. Among over 2000 unique eukaryotic protein kinases, protein kinase A (PKA)[1] is the most intensively studied and the best understood biochemically. PKA thus serves as a prototypical enzyme for the whole family.

Within the cell, PKA is typically stored as an inactive holoenzyme complex comprised of two regulatory (R) and two catalytic (C) subunits (*3*, *5*). Two functionally nonredundant types of R-subunits, RI and RII, define the variety of responses of PKA to extracellular signals. In the holoenzyme complex, RI subunits position an inhibitor peptide in place of substrate in each C-subunit loaded with an ATP molecule and two Mg^{2+} ions. Inhibition is allosterically lifted upon binding of four cAMP molecules to the two R-subunits, one to each of the tandem cAMP-binding domains, thereby unleashing the active C-subunits. In addition to allosteric activation by cAMP, ATP and Mg^{2+} concentrations are important for association between the C- and RI-subunits (*3*, *8*, *9*). RII-subunits differ from RI in that they provide true substrate peptide and do not require either Mg^{2+} or ATP to form a holoenzyme complex.

ATP and Mg^{2+} bind to PKA in the active site cleft between the small and large lobes (see Figure 1). A flexible Gly-rich loop from the small lobe closes over the nucleotide like a lid, sealing off the active site (*10*−*17*). Main chain NH groups of three residues, S53, F54, and G55, at the tip of the Gly-rich loop form the so-called nest that latches to the phosphates (Figure 1B) (*18*, *19*). This interaction helps to lock the enzyme in the closed conformation and to properly position the nucleotide for catalysis (*13*, *14*, *20*−*22*). Inside the active site, a conserved K72-E91-D184 triad reorganizes to bind the nucleotide with Mg^{2+} ions by breaking the K72-D184 salt bridge. The K72 side chain coordinates α- and β-phosphates, while D184 coordinates the Mg^{2+} ions. In addition, another residue K168 coordinates γ-phosphate to further stabilize the nucleotide-PKA complex.

The binding site can accommodate two Mg^{2+} ions (Figure 1) (*20*, *23*, *24*), the final coordination of which depends on the bound nucleotide. With ATP, one Mg^{2+} ion, referred to as activating, is chelated by the β- and γ-phosphates, and coordinates the D184 side chain from the K72-E91-D184 triad in a bidentate fashion (*24*, *25*). The second Mg^{2+} ion, termed inhibitory, binds to the α- and γ-phosphates, a single carboxyl oxygen of D184, and a side chain carbonyl oxygen of N171. Structural water molecules complete coordination shells of each

†This work was in part supported by grants from NIH, NSF, NBCR, CTBP, and HHMI, including NIH Grant GM19301.

*Corresponding author. Address: University of California, San Diego Urey Hall, Room 4206, 9500 Gilman Dr. M/C 0365, La Jolla, CA 92093-0365. E-mail: ikhavru@mccammon.ucsd.edu. Tel: (858) 366-3090. Fax: (858) 534-4974.

[1]ATP, adenosine triphosphate; ADP, adenosine diphosphate; DNA, deoxy-ribonucleic acid; PKA protein kinase A; HFB, harmonic Fourier beads; cAMP, cyclic adenosine monophosphate.

 Published on Web 11/03/2009

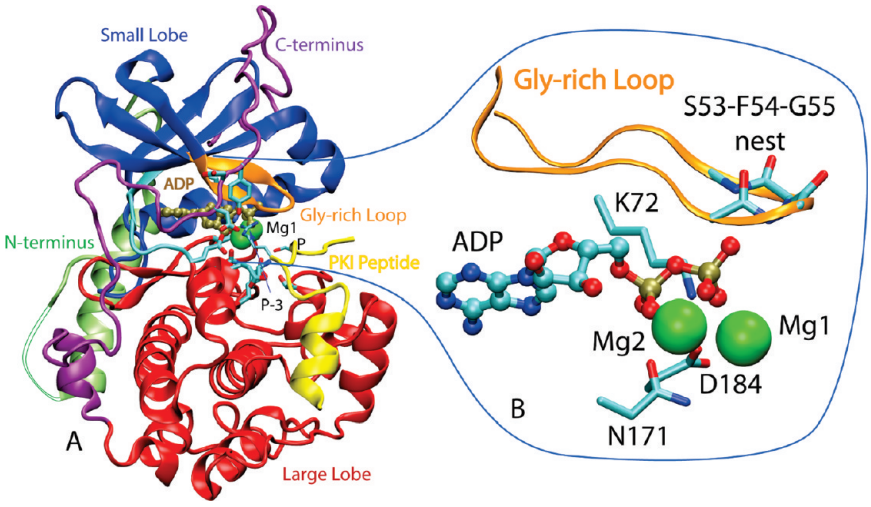

FIGURE 1: The depicted model of the catalytic subunit of PKA was derived from the transition state analogue structure with the PDB code 1L3R by removing AlF_3. (A) The small and large lobes of the conserved catalytic core are shown using cartoon representation in blue and red, respectively. PKA-specific N-terminal and C-terminal tails are depicted in lime and purple, with the hollow segment showing disordered residues. The Gly-rich loop in the small lobe is shown in orange. The inhibitor peptide PKI is depicted in yellow. This peptide was removed in our simulations. Two Mg^{2+} ions are shown as green balls. Mg1 corresponds to activating, whereas Mg2 corresponds to inhibitory ion. The ADP molecule is shown in tan ball-and-stick model. A few side chains that are most sensitive to Mg^{2+} presence in the active site are shown using licorice representation. On the PKI inhibitor the phosphorylation site and the P-3 Arg are also shown in thinner licorice. (B) A close up of the ADP and Mg^{2+} ions bound in the active site.

ion to an octahedron (*26*). Upon transfer of the γ-phosphate to substrate followed by release of the phosphopeptide, the coordination shells of the two Mg^{2+} ions rearrange to adjust to the ADP product as has been shown by crystallographic (*25*) and computational (*27*−*31*) studies. In the product state with ADP, the activating Mg^{2+} ion coordinates only the β-phosphate, whereas the inhibitory ion binds α- and β-phosphates.

The binding site for the activating Mg^{2+} has a higher affinity (K_d = 1.7 mM) than the inhibitory site (K_d = 3.2 mM) with ATP (*32*, *33*). In contrast, with ADP, the two Mg^{2+} binding sites have identical binding constants (K_d = 1.6 mM) (*34*). Therefore, depending upon Mg^{2+} concentration, PKA can have ATP bound with either a single activating ion or both activating and inhibitory ions. Interestingly, it is only when the second Mg^{2+} ion is bound that all of the residues and the phosphates at the active site cleft become ordered and could be resolved crystallographically (*24*). Binding a Mg^{2+} ion in the primary site is believed to activate, whereas binding an additional Mg^{2+} ion in the secondary site is believed to inhibit catalysis (*32*−*37*). Why would the second, low affinity Mg^{2+} ion that brings order into the active site cause catalytic inhibition?

At low Mg^{2+} concentrations PKA has been inferred to undergo conformational change following binding of the nucleotide. This conformational change can be partially rate limiting (*33*, *37*). Although details of the conformational change are unavailable, one hypothesis is that it involves rearrangements of various residues in the active site along with the Gly-rich loop and the binding cleft (*20*). Another prominent hypothesis involves a highly conserved DFG motif. On the basis of the universal conservation of these residues in the kinase family and their link to kinase inactivation (*38*), it was suggested that conformational changes in this region may facilitate the release of ADP (*39*, *40*).

At high Mg^{2+} concentrations, when both Mg^{2+} are bound, kinetic studies have identified ADP release to be the rate-limiting step in PKA catalysis (*36*, *37*, *41*−*45*). It is not known whether Mg^{2+} ions release simultaneously with or prior to ADP dissociation. Although the activating Mg^{2+} ion is necessary and sufficient for catalysis, the second Mg^{2+} ion increases the nucleotide binding affinity to PKA (*32*, *34*, *46*, *47*). In fact, binding of either ATP or ADP to PKA critically depends on Mg^{2+} ions (*23*, *32*, *34*, *35*, *47*). Neither nucleotide nor Mg^{2+} ions alone bind strongly to PKA, whereas together their binding affinities increase substantially. The reasons for this cooperativity remain unclear.(*23*) Thus, Mg^{2+} ions play crucial roles at various stages of PKA catalysis and inhibition and are worth studying in detail (*8*, *9*, *23*, *32*−*37*, *46*, *47*).

Answering the questions about how Mg^{2+} ions affect PKA catalysis in general, and in particular at the critical, rate-limiting step of ADP release would require atomically detailed structural and energetic description of the process, which is difficult to achieve experimentally. Computational methods, on the other hand, can provide such a description in principle. The first direct computational study of the ADP release mechanism was performed in earlier work from our lab that employed steered molecular dynamics (SMD) (*48*−*50*) to pull ADP out of the binary complex with PKA (*51*). This work showed that the adenine ring underwent a swinging motion out of the active site while the pyrophosphate remained anchored to the Gly-rich loop. The Gly-rich loop opened significantly during this rearrangement and eventually allowed the release of the pyrophosphate. Although this pioneering work provided important insights into the mechanism of ADP release, it suffered from a series of shortcomings. No free energy estimates were provided. Most importantly, the Mg^{2+} ions were absent from the simulations and hence their role could not be established.

Here we investigate in detail the effect of Mg^{2+} ions on the rate-limiting step of ADP release from PKA. Previous studies identified the need for ensemble methods to study transitions in large molecules such as PKA (*27*−*31*, *51*−*53*). Therefore, we model the ADP release transition directly by computing a transition path ensemble that takes an ADP molecule from a bound state to a well-separated state in which ADP no longer interacts with PKA. To do that, we employ an equilibrium transition path ensemble methodology, namely, harmonic

Fourier beads (HFB) (*54*−*58*). The HFB method, in addition to its capability of finding minimum free energy transition path ensembles, can compute corresponding free energy profiles and their decompositions. Such energy partitioning is invaluable for understanding of the ligand binding mechanism, and is impossible to obtain experimentally. By computing the transition path ensemble and their free energy characteristics in the presence and absence of Mg^{2+} ions, we probe the role of the Mg^{2+} directly for the first time.

Thus, the present study provides a detailed structural and energetic description of the complete mechanism of ADP binding and release. The results allow us to evaluate previous proposals for the conformational changes that should facilitate ADP release, such as Gly-rich loop opening and DFG-flip. Furthermore, the free energy data reveals the contributions of individual nucleotide groups and Mg^{2+} ions to the nucleotide binding. It reveals the origin of binding cooperativity between the Mg^{2+} ions and the nucleotide, and demonstrates that Mg^{2+} ions act as linchpins that fasten the nucleotide in the active site seat.

METHODS

The HFB Method. We employ the recently developed HFB transition path ensemble optimization and free energy calculation method (*54*−*58*). Details of the approach have been presented elsewhere. Briefly, the HFB method requires the initial reactant and product states of the system to be predefined. Intermediate states are then generated by an adaptive Fourier interpolation and represented together with the reactant and product as a finite set of structures, termed beads. The corresponding Cartesian coordinate space is then partitioned into a reactive coordinate space (RCS) that best describes a particular transition and a complementary spectator coordinate space (SCS). Independent classical molecular dynamics simulations of each bead with matching harmonic restraints on RCS positions are used to compute the Cartesian free-energy gradients or mean forces using the generated ensemble. These mean forces are used to drive the enhanced steepest descent optimization of all beads (representing the transition path ensemble) toward the bottom of the nearest free-energy valley. Finally, a Fourier interpolation of the mean forces is used to compute the potential of mean force (PMF) along the path via a line integral approach.

Initial Path Setup. To set up a transition path ensemble optimization, one needs to define a reactant and a product state for the ADP dissociation process. Reactant state setup proceeded from the crystallographic structure of the transition state analogue, PDB code: 1L3R, by removing AlF_3 and the phosphorylated substrate peptide. This resulted in a catalytic subunit complexed with two Mg^{2+} ions and an ADP molecule. Missing residues, numbers 5 through 13, were modeled (see Supporting Information). Histidine residues 62, 68, 87, 142, 158, and 260 were doubly protonated, while histidines 131 and 294 were protonated on their Nδ atoms only. In addition, residues S10, S139, T197, and, S338 were phosphorylated, each contributing −2 charge. To maintain system neutrality and near physiological ionic strength 31 Cl^-, 23 Na^+ and 4 Mg^{2+} ions were placed in a rectangular simulation box of 79 × 88 × 69 Å filled with 13 103 water molecules. The total number of atoms in the simulation box was 45 142.

To generate the product state we modified the reactant state by translating ADP 33 Å to a corner of the simulation box along a direction that visually presented the least steric clashes. Note that the two Mg^{2+} ions bound at the active site were not immediately translated along with the ADP (see below).

To establish a sound coordinate system for the path activation and subsequent optimization, we performed analysis of available PKA crystallographic structures (see Supporting Information) using Bio3D software (http://mccammon.ucsd.edu/~bgrant/bio3d) (*59*) . This analysis identified four helices in the large lobe as the least mobile between available structures. This rigid core comprised residues 140−160, 217−234, 263−274, and 288−298 from helices E, F, H, and I, respectively. The rigidity of these helices has also been noted in previous molecular dynamics simulations and structural analyses (*15*, *60*). These core positions were kept fixed throughout the simulations and served as the reference for alignment of beads during the transition path activation and optimization procedure. In particular, every time a new path was generated, reference beads were realigned to match the core Cα atoms of the 1L3R PDB structure.

Activated Evolution. We followed a standard activated evolution procedure to build the path between the reactant and the product states (*58*). Specifically, we used 24 beads and a soft mass-weighted force constant of 0.05 kcal/mol/Å^2 on all heavy atoms of the solute excluding fixed atoms of the core. Hence, the RCS comprised all nonfixed heavy atoms of the protein, ADP and bound Mg^{2+} ions (hereafter termed RCS1). Activation started from the reactant state with a new bead activated after every evolution step with 50 ps of MD. This procedure was continued for each of the 24 beads. During the procedure, once activated, a bead continues to evolve until the final step when all beads are active.

To probe the behavior of the Mg^{2+} ions upon ADP dissociation, we designed our activated evolution procedure to initially bias the ions to their original crystallographic positions. That is, similar to the reactant sate, our first product state had both Mg^{2+} ions bound to their original positions in the active site. After running activated evolution for 20 steps, we observed that in all cases Mg^{2+} ions closely followed the dissociating ADP despite the opposing bias. We then altered the product state by translating the Mg^{2+} ions by the same amount as ADP. This prevented collapse of the Mg^{2+} ions back to the bound state at the product beads. With that we completed the activated evolution procedure with four final steps. As a result, in the product state the Mg_2ADP moiety was in a conformation similar to the bound state, but simply translated outside the active site.

Transition Path Optimization and PMF Calculations. After the initial path was generated, we continued optimization for 451 more optimization steps, while gradually expanding the path to 185 beads. Near the end of optimization, the RCS1 has been reduced to include only heavy backbone atoms of the protein, select atoms of ADP and coordinated Mg^{2+} ions (RCS2). The details of the optimization and changes in RCS are also provided in Supporting Information.

Because optimization of an analogous path without Mg^{2+} ions would have been prohibitively expensive, we devised the following procedure to assess the influence of Mg^{2+} ions on the ADP binding. We used the coordinates of the final path optimized with Mg^{2+} ions, but translated the bound Mg^{2+} ions to two different corners of the simulation box where they were held by the restraints and interacted only with the solvent. The resulting perturbations of all the atoms affected by the move were then gradually relaxed and the system re-equilibrated for all the beads prior to final data collection and PMF calculation.

To allow more robust PMF calculations, we further reduced the reactive coordinate space to include only core Cα atoms along with ADP and Mg^{2+} ion coordinates (hereafter termed RCS3). The final PMFs for the 185-bead paths with and without Mg^{2+} ions were computed using RCS3 with a force constant of 5.0 kcal/(mol Å^2). The collection time for each bead was 1 ns. The integration of the PMFs employed the maximum number of Fourier basis functions, which equals the total number of beads in the path.

Advantageously, the HFB method allows decomposition of the free energy along the path onto subsets of the RCS degrees of freedom. Here, we decomposed the final PMFs into contributions from both Mg^{2+} ions and the three groups of ADP, namely, the adenine, ribose ring, and the pyrophosphate, both individual and collective. Integrating the degrees of freedom of the rigid protein core that were restrained to the 1L3R crystallographic coordinates throughout the path must give a flat PMF, and can be used as an internal standard.

Estimates of Systematic Errors in PMFs. To gauge possible systematic errors in the final PMFs, and to accurately estimate the deformation of the ADP ligand upon binding to the protein, we constructed two additional ADP-only paths for PMF calculations. For the first path, we extracted the coordinates of the ADP molecules from the optimized path for the whole system and then translated their RCS3 centers of mass to the origin. For the second path, we used a line interpolation procedure to generate a much shorter, 12-bead path between the translated reactant and product ADP states that were quite similar. The 12-bead path should yield accurate free energy difference between the end point states, thus, serving as a benchmark. Each translated ADP molecule was solvated in a small cubic box of dimensions of 31 × 31 × 31 Å filled with 991 water molecules, 5 Na^+, and 2 Cl^- ions. Following equilibration, we collected data for 4 ns per bead using restraints on the ADP atoms as defined in the RCS3. The final PMFs allowed error evaluation of the PMF integration and the free energy of deformation of the ADP upon binding to PKA.

Simulation Parameters. For the transition path optimization and PMF calculations, we used the HFB method as implemented in the CHARMM simulation package (version c34b2) (*61*). MD simulations were performed with NAMD (version 2.6) (*62*) using the CHARMM27 forcefield (*63*, *64*). The temperature was maintained at 310 K with the Langevin thermostat using a coupling parameter of 1 ps^{-1}. Pressure was maintained at 1 atm by the Nosé-Hoover Langevin piston method with a piston oscillation period of 200 fs and a piston decay parameter of 500 fs (*65*, *66*). Nonbonded interactions were computed using particle mesh Ewald (*67*, *68*) with a 8.5 Å real space cutoff for electrostatic interactions and a switching function between 8.5 and 10 Å for vdW interactions. However, a multiple time-step method (*69*, *70*) was employed for the electrostatic forces with full electrostatic interactions computed every other step. The nonbonded interaction list was updated every 20 steps using a 12 Å cutoff. Covalent bonds involving hydrogen atoms were constrained using SHAKE (*71*−*73*) with a tolerance in the bond length of 10^{-8} Å. The MD integration step size was 2 fs.

RESULTS

Energetics of ADP Release. Calculating free energy profiles along the optimized transition path yields detailed information on the overall ADP association free energy and the forward and reverse activation barriers. In addition, decomposition of the free energies into contributions from specific subgroups of atoms permits a deeper understanding of the mechanism of ADP release from PKA. It should be noted that the computed free energies are properties of our model and underlying forcefield. Furthermore, the computed free energies have not been converted to the standard binding free energies as this requires a nontrivial correction (*74*−*80*) that is presently unavailable for the multidimensional restraints employed in the present study. Therefore, the computed free energy values should not be compared directly to experimental values. Instead, trends should be inferred to generate testable hypotheses.

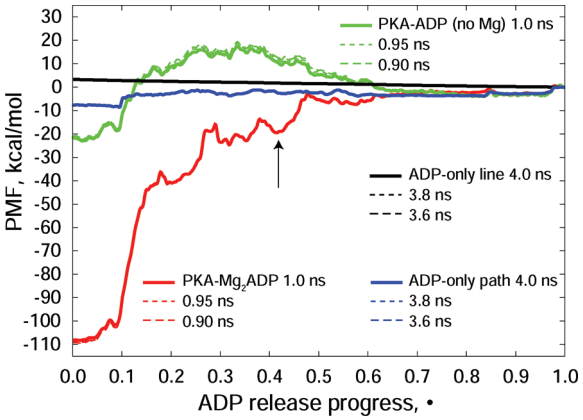

FIGURE 2: The final PMFs for ADP binding to PKA and ADP deformation induced by the binding. The free energy of the unbound state is set to zero. The line interpolated ADP-only PMF used 12 beads; all the other PMFs employed 185 beads. The PMFs were collected on the RCS3 surface (see Supporting Information). The ADP-only PMFs for free energy of deformation have been collected with total of 4.0 ns MD per bead. The PMFs for ADP binding to PKA have been computed using 1 ns MD per bead. In addition to the final PMFs, two intermediate PMFs are shown to demonstrate convergence. The arrow points to the metastable intermediate at α = 0.42. All the PMFs correspond to 1 atm and 310 K.

Error Estimates. Transition path optimization yields a relatively rough path even with 185 beads. It is anticipated that PMF integration along such a rough path may suffer from systematic errors. To assess these errors, we computed ADP-only PMFs for the ADP deformation due to binding PKA. In particular, we compare the free energy along the extracted 185-bead path with that from a 12-bead path constructed by linear interpolation between the same end points.

Because both paths have the same end points, they should yield the same ADP deformation free energies in the absence of systematic errors. The free energy from the linearly interpolated 12-bead path is expected to be the most accurate and should serve as a benchmark. The final ADP-only PMFs appear rather smooth and well converged. (Figure 2). However, the 185-bead PMF exhibits two kinks due to abrupt changes in the ribose ring puckering between beads 19 and 20 that correspond to the release progress variable α = 0.10 and also between beads 180 and 181 at α = 0.98.

The linearly interpolated benchmark path yields a 3.3 kcal/mol ADP deformation free energy (see Table 1). In contrast, the deformation free energy calculated along the coordinates extracted from the path optimized for the full system produces −7.5 kcal/mol. Thus, the absolute error in PMF calculation along the 185-bead path is 10.8 kcal/mol. Therefore, we can

Table 1: Total Free Energies (in kcal/mol) and Their Decompositions into Specific Groups for ADP-Binding to PKA, along with ADP Deformation Benchmarks[a]

	Total	TotalC[b]	Mg1Mg2	Mg1	Mg2	ADP	A	P	R
ADP-line	3.3	3.3							
ADP-path	−7.5	3.3							
ADP-2Mg	−108.1	−97.3	−33.3	−12.7	−20.6	−74.8	−32.5	−24.7	−17.5
ADP-0Mg	−22.0	−11.2	0.0			−22.3	−33.1	58.8	−48.1
2Mg-0Mg	**-86.1**	**-86.1**	**-33.3**			**-52.5**	**0.6**	**-83.6**	**30.5**

[a]ADP-line is the 12-bead ADP-only linearly interpolated path that provides the free energy of ADP deformation upon binding to PKA. This free energy serves as a benchmark and is used to correct the total binding free energies. All the other values are given for 185-bead paths. ADP-path is ADP-only path extracted from the optimized path for ADP release from PKA in the presence of two Mg^{2+} ions. ADP-2Mg and ADP-0Mg are the free energies computed for the full system along the optimized ADP release path with Mg^{2+} ions and after the ions have been removed without reoptimization, correspondingly. A − adenine, P − pyrophosphate, R − ribose. [b]Corrected for the systematic error.

expect that the magnitude of the association energies calculated for the full system would be overestimated by at least 10.8 kcal/mol. We will use this estimate of the systematic error to correct the final free energy differences obtained for the full system. Where applicable, the corrected free energy differences will be shown in parentheses.

ADP Release PMFs. As the final PMFs in Figure 2 demonstrate, association of the Mg_2ADP with PKA is favorable by −108.1 (−97.3) kcal/mol and has no significant barriers. In the absence of Mg^{2+} ions, ADP association remains favorable by as much as −22.0 (−11.2) kcal/mol, but has a significant barrier of 17.5 kcal/mol. Although in the absence of Mg^{2+} ADP release faces a significant barrier of 39.5 kcal/mol, it is much less unfavorable than release with Mg^{2+} ions. Note that the path ensemble for ADP release in the absence of Mg^{2+} ions has not been free energy optimized. Therefore, the referred barriers provide upper bounds for the true barriers.

ADP Release Free Energy Decomposition. Although the overall association free energies and corresponding free energy barriers are useful, they provide little insight into the mechanism without further structural analysis. Additional details about the mechanism of ADP release from PKA can be gleaned from free energy decomposition analysis. Such analysis would reveal exactly how Mg^{2+} ions affect ADP release. Advantageously, the fact that we used the same path to compute PMFs in the presence and absence of Mg^{2+} ions greatly simplifies the comparison of free energy decompositions.

ADP Release with Mg^{2+} Ions. Decomposition of the PMF for ADP release in the presence of two Mg^{2+} ions (Figure 3A and Table 1) reveals individual contributions of different groups. The ADP itself contributes −74.8 kcal/mol to the overall association free energy. Breaking the ADP contribution further into those from adenine, ribose, and the pyrophosphate groups, we find contributions of −32.5, −17.5, and −24.7 kcal/mol, respectively. Note that all three groups contribute favorably to association. The two Mg^{2+} ions contribute −33.3 kcal/mol to the total association free energy. Interestingly, activating Mg1 contributes −12.7 kcal/mol, whereas inhibitory Mg2 contributes a significantly larger amount of −20.6 kcal/mol. The control contribution of the restrained protein core degrees of freedom alone yields 0.0 kcal/mol as anticipated.

ADP Release without Mg^{2+} Ions. Decomposition of the PMF obtained without Mg^{2+} ions (Figure 3B and Table 1)

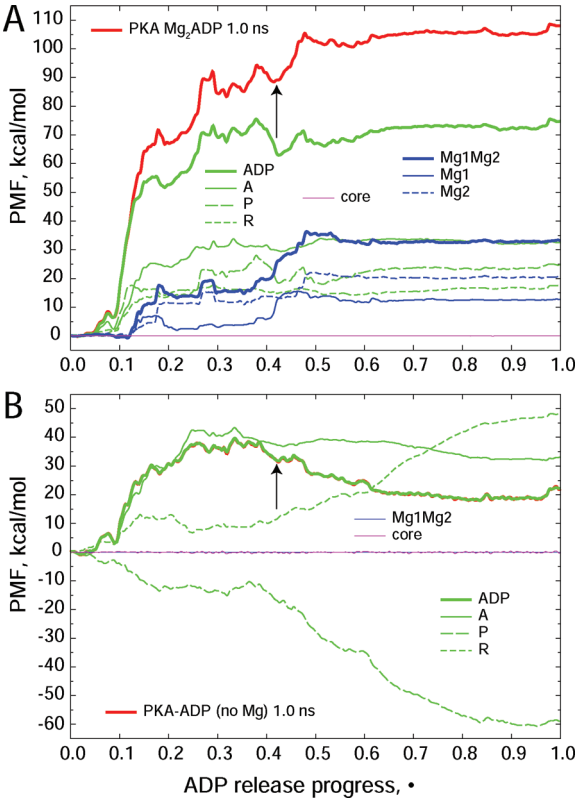

FIGURE 3: Decomposition of the PMFs for ADP binding to PKA with (A) and without (B) Mg^{2+} ions. The complete PMFs are shown in red thick solid lines. The arrows point to the location of the metastable intermediate at $\alpha = 0.42$ that only exists with Mg^{2+} ions. The overall ADP contribution is shown in green thick solid line. Its further decomposition into contributions from adenine ring (A), ribose (R), and pyrophosphate (P) are shown in thin lines of the same color. In the case where Mg^{2+} ions are present, their overall contribution is shown in blue solid thick line whereas the individual contributions are shown in thin lines of the same color. Also shown in thin purple and blue lines are the control contributions of the protein core degrees of freedom and of the two Mg^{2+} ions, respectively.

highlights the pronounced influence of Mg^{2+} ions on the ribose and the pyrophosphate groups of ADP. In the absence of Mg^{2+} ions, ADP is the sole contributor to the association free energy. It contributes −22.3 kcal/mol, which is significantly (by 52.5 kcal/mol) weaker than in the presence of Mg^{2+} ions. Interestingly, the adenine ring makes a favorable contribution of −33.1 kcal/mol that is nearly identical to that in the presence of the Mg^{2+} ions (−32.5 kcal/mol). This similarity suggests independence of the adenine association with PKA from Mg^{2+} ions. Importantly, removal of the Mg^{2+} ions greatly perturbs the contributions from the ribose and the pyrophosphate groups in the opposite directions. In particular, the negatively charged phosphate group strongly disfavors binding by as much as 58.8 kcal/mol. The ribose contribution is favorable by −48.1 kcal/mol, but falls 10.7 kcal/mol short of canceling the pyrophosphate contribution. As expected, the two control contributions, namely, that of the protein rigid core and of the separate Mg^{2+} ions yield numbers very close to zero (0.0 and 0.3 kcal/mol, respectively).

Structural Changes in PKA Associated with ADP and Mg^{2+} Release. We have analyzed atomic contacts established between the ADP, Mg^{2+} ions and PKA along the ADP binding path. The results are summarized in Table 2S of Supporting Information. Here we report only the most interesting results.

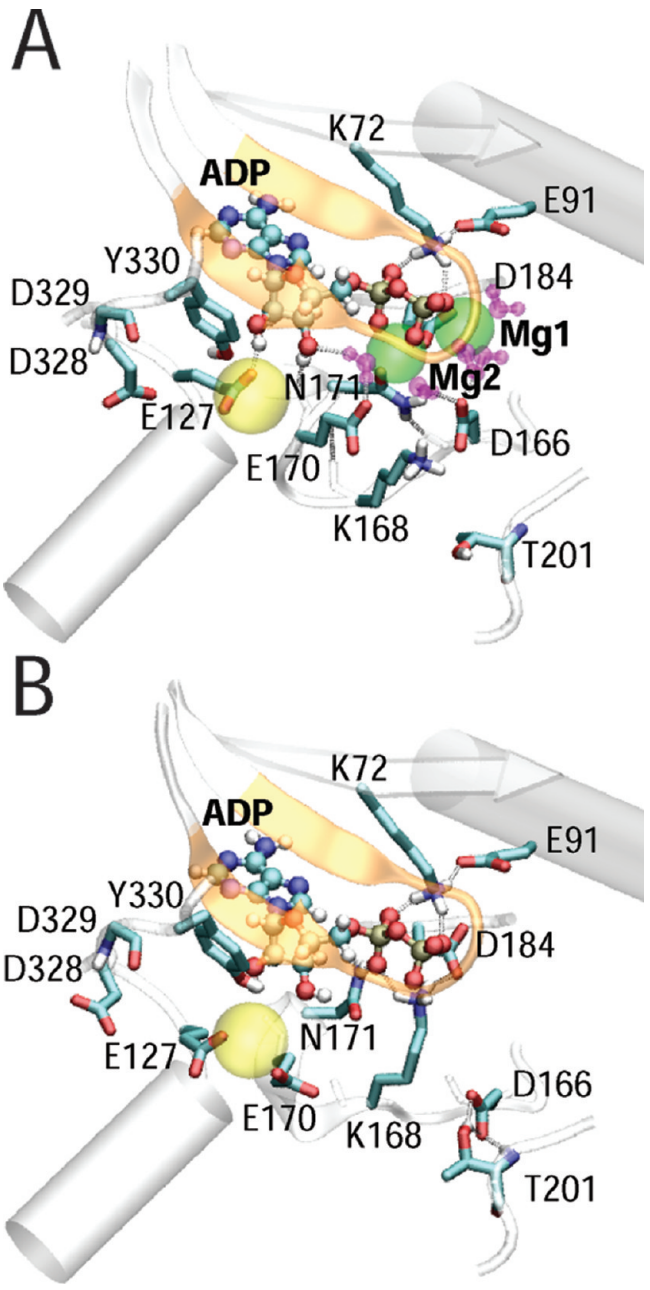

FIGURE 4: A snapshot from an optimized reactant state ensemble: the active site of the PKA with ADP bound with (A) and without (B) two Mg^{2+} ions. The Gly-rich loop is shown in cartoon representation in transparent orange color. All the other secondary structure elements of the protein frame that are relevant to the active site are shown in transparent white-gray. The ADP is shown with ball-and-stick model. The important active site residues are depicted in licorice representation. The two Mg^{2+} and one Na^{+} ions are shown in green and yellow transparent balls, respectively. Water molecules coordinating Mg^{2+} ions are shown in transparent pink color. Some of the hydrogen bonds present are depicted with dashed bonds.

Because two functionally distinct Mg^{2+} ions can be present in the active site, we distinguish them based on their coordination environment in the reactant state. The coordination sphere of Mg1 is comprised of the β-phosphate of the nucleotide and the carboxyl group of D184, in a bidentate coordination mode. Three additional water molecules complete the coordination shell of Mg1. The coordination sphere of Mg2 comprises the α- and β-phosphates of the nucleotide, a single carboxyl oxygen of D184, the side chain carbonyl of N171 along with two additional water molecules (Figure 4A). Hence, each Mg^{2+} ion has a total of six coordinate bonds in a roughly octahedral coordination shell.

Structural Observations Based on the End-States. Because transition path optimization also optimizes the end-states, namely, reactant and product, that are experimentally observable, it is worth analyzing structural changes in these states first. The reactant state corresponds to a binary complex of PKA with ADP (*20*), whereas the product state corresponds to the apo enzyme (*22*). To the best of our knowledge, no structure of the binary complex with ADP is currently available. To date, all the structures with ADP include a bound peptide and therefore recruit some of the key residues near the active site for peptide binding. Although the crystal structure of the apo enzyme has been solved, many of its key residues are disordered. In addition, these structures are perturbed to some degree by crystal contacts (*21*). Therefore, our work provides a look at the binary complex and the apo enzyme in solution from the point of view of classical MD simulations.

PKA Response to Substrate Removal. Because our reactant state was derived from the ternary complex (PDB code: 1L3R) by removing the phosphorylated substrate peptide, we have an opportunity to trace spontaneous rearrangements of key residues that were previously involved in protein−protein interactions with the substrate. Thus, we observed the residue E170 that coordinated P-2 Arg of the substrate (*81*) to flip up toward the nucleotide to make a salt bridge with K168. The residue E127 that together with Y330 coordinated P-3 Arg (*81*) remained relatively unperturbed. However, Y330 and its adjacent cluster of residues F327, D328, and D329 from the C-terminal tail moved away from E127 upon substrate removal.

Further comparison of the reactant and product structures with and without Mg^{2+} ions highlighted residue clusters important for interactions of PKA with ADP and residues sensitive to the presence of Mg^{2+} ions.

Mg^{2+}-Dependent Rearrangement of the D184-K72-E91 Triad. The conserved residues D184, K72, and E91 are located in close vicinity to the adenine binding site. In the product state (formed upon dissociation of both ADP and Mg^{2+} ions from PKA) these residues participate in two salt bridges, namely, D184-K72 and K72-E91 (Figure 5A,B). Breaking the D184-K72 salt bridge upon ADP association engages the K72 side chain in interactions with the pyrophosphate and D184 in interactions with both Mg^{2+} ions (Figure 4A). As a result, sacrificing the D184-K72 salt bridge creates four new salt bridges: two involving K72 with the α- and β-phosphates of the nucleotide, and two resulting from the bidentate coordination of Mg1 with D184. D184 contributes an additional salt bridge in the presence of Mg2. In the absence of ions only two salt bridges, between K72 and the phosphate groups are possible (Figure 4B). In this case, the negative charge on the D184 creates an unfavorable repulsive interaction with the negatively charged phosphate group. This repulsion can be rescued by K168 residue from another important triad.

The Effect of Mg^{2+} on the N171-D166/K168 Interactions. In the ADP bound reactant state with two Mg^{2+} ions, the carbonyl of residue N171 coordinates Mg2, while its amide coordinates the backbone carbonyl of D166 (Figure 4A). Removing Mg^{2+} ions from the active site disrupts the hydrogen bonding of N171 with D166, and allows the N171 amide to flip toward and hydrogen bond the α-phosphate of ADP (Figure 4B). Moreover, the carbonyl of the unleashed N171 can participate in hydrogen bonding with either the 3′-OH of ADP or the side chain

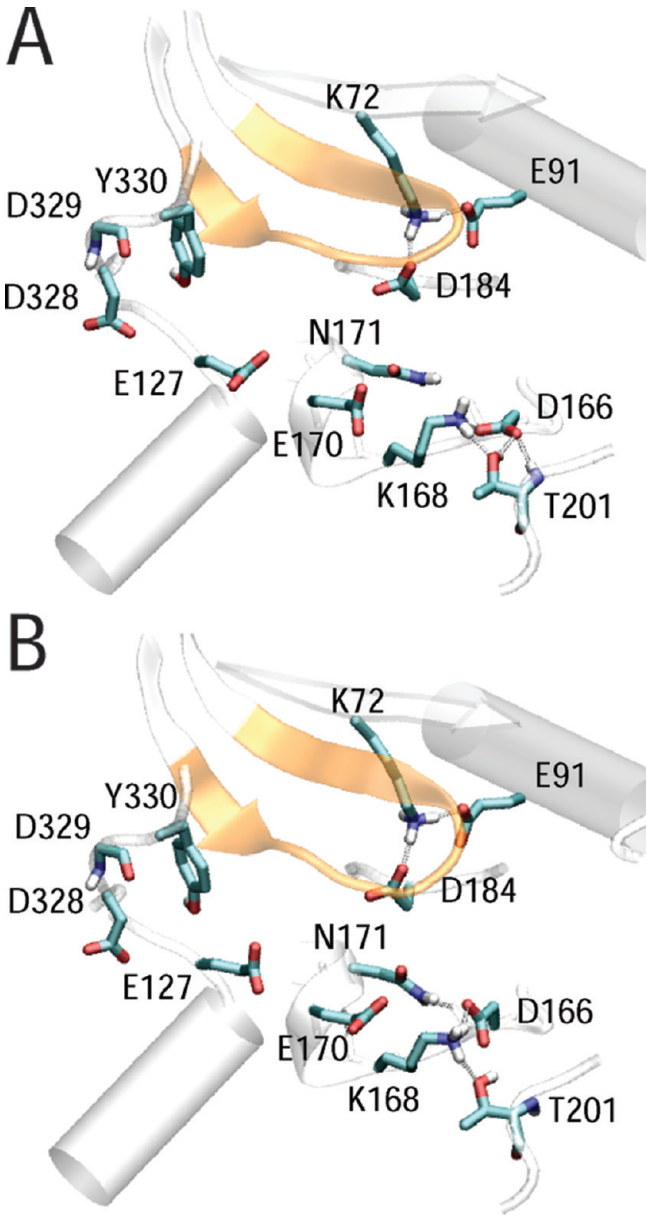

FIGURE 5: A snapshot from an optimized product state ensemble: the empty active site of the PKA formed upon release of ADP with (A) and without (B) Mg^{2+} ions. The Gly-rich loop is shown in cartoon representation in transparent orange color. All the other secondary structure elements of the protein frame that are relevant to the active site are shown in transparent white-gray. The important active site residues are depicted in licorice representation. Some of the hydrogen bonds present are depicted with dashed bonds.

of K168. Removing ADP from the binding pocket relaxes the N171 side chain back to its original state hydrogen bonding to the backbone of D166 (Figure 5A,B) (*22*, *24*).

The K168-D166-T201 Triad. The residue K168 is part of yet another important Mg^{2+}-sensitive cluster, K168-D166-T201. The catalytic base D166 resides in the immediate vicinity of the Mg^{2+} ions, contacting water molecules in their primary coordination shells (Figure 4A). Interestingly, removing both Mg^{2+} ions, while keeping the ADP bound, triggers a local conformational change of the D166 side chain that assumes a position suitable for coordination with T201 (often in a bidentate mode, with one hydrogen bond to the backbone amide and the other to the side chain OH group) (Figure 4B). Furthermore, the excess negative charge on ADP triggers another conformational change during which K168 breaks away from its binding partners, E170 and D166, and moves to coordinate the phosphates of ADP (Figure 4B). Once the nucleotide molecule leaves the binding site, D166 coordinates primarily the side chain of T201 (Figure 5A,B). In addition, D166 forms a strong salt bridge with the side chain of K168 released by the nucleotide. Thus, the residues K168, D166, and T201 form yet another versatile functional triad.

A Third High Affinity Cation-Binding Site in the Reactant State. ADP association with PKA creates two well-established binding sites for Mg^{2+} ions. These sites are not accessible to Na^+ ions during our simulations with Mg^{2+} ions removed from the active site. Note that Na^+ ($R = 0.95$ Å) is larger than Mg^{2+} ($R = 0.65$ Å) and cannot always penetrate places that Mg^{2+} can. In addition to these two sites, analysis of the 3D-distribution of Na^+ ions around the surface of PKA identified a third high-affinity cation-binding site. This site exists only in the presence of ADP and involves its 2′-OH group along with the side chains of residues E127 and Y330. Binding of a Na^+ ion to this third site is stronger than to phosphorylated side chains with twice the negative charge.

ADP Release Trajectory. In the path optimized with Mg^{2+}, we observe that the adenine group swings out of its binding pocket followed by the ribose and the pyrophosphate groups. Mg^{2+} ions remain associated with ADP, thus leaving the active site together with the nucleotide. Because we did not optimize the ADP release path in the absence of Mg^{2+} ions, we do not know how removing Mg^{2+} ions would affect the actual trajectory for the ADP release. Nevertheless, we can use previous SMD simulations from our lab for comparisons (*51*). Furthermore, as will be shown in the Discussion, dissecting PMFs into contributions from adenine, ribose, and pyrophosphate allows speculations on the order of events in the absence of Mg^{2+} ions. At this point, we recall that the pyrophosphate group that serves as an anchor with Mg^{2+} ions strongly favors ADP release once the Mg^{2+} ions are removed.

Transport of Ions by Carboxylate Shifts. As mentioned above, our optimized transition path ensemble has the two Mg^{2+} ions remaining closely associated with the ADP during the release. Given that in generating the initial path we intentionally biased the Mg^{2+} ions to stay in the active site, this behavior strongly suggests that the interactions of both Mg^{2+} ions with ADP are much stronger than with PKA. Because during the path optimization the Mg^{2+} ions are subject to harmonic restraints, they are not free to dissociate from ADP. Whether this is a feasible transition path can be decided based on its free energy profile.

Assuming that the ions would remain associated with ADP, the optimized transition path ensemble indicates that release or, reversibly, binding of nucleotide associated Mg^{2+} ions would proceed in highly orchestrated stepwise manner (see Supporting Information for details). Two conserved residues, E170 and D184, participate in a Mg^{2+} release relay involving a series of carboxylate shifts (*82*−*86*). Although we have computed the path for ADP release, it is more instructive to consider the reverse process of binding in describing the relay. Residue E170 acts like a fishing rod that tethers and directs the incoming Mg^{2+} ions into the active site. D184, from the conserved triad of D184-K72-E91, receives the two Mg^{2+} ions at the end of the relay.

On-Path Intermediate. The final PMFs identified a metastable intermediate in the presence of Mg^{2+} ions that is largely absent otherwise (Figure 6A,B). Structural analysis reveals that this intermediate, located at the ADP release progress variable

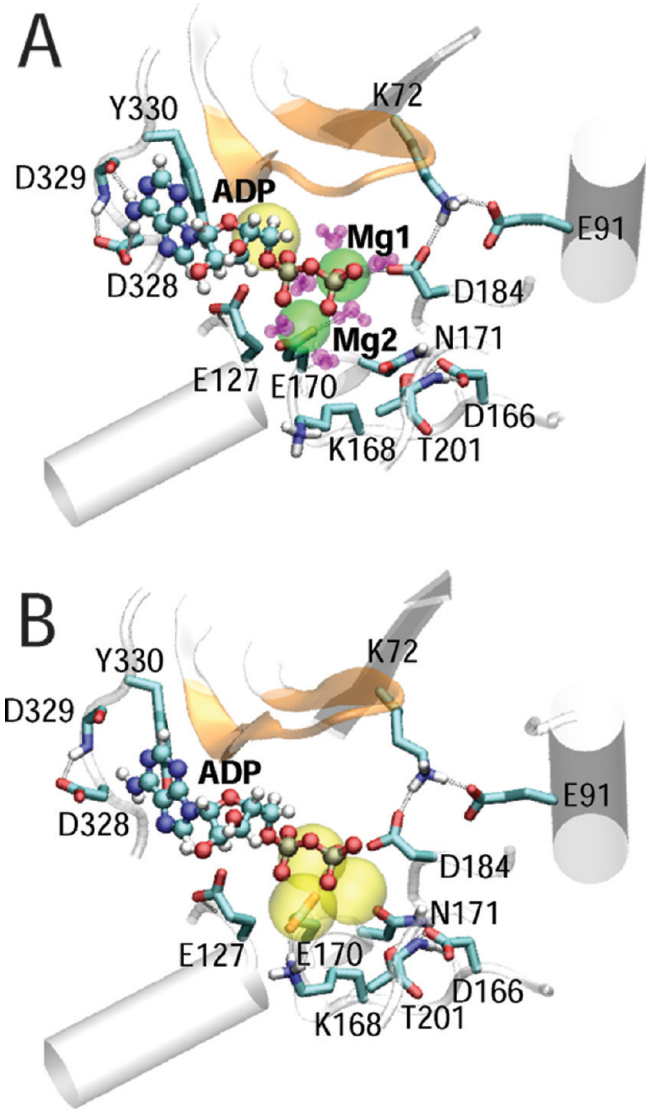

FIGURE 6: A snapshot from an optimized intermediate state ensemble: the active site of the PKA during ADP release with (A) and without (B) Mg^{2+} ions. The Gly-rich loop is shown in cartoon representation in transparent orange color. All the other secondary structure elements of the protein frame that are relevant to the active site are shown in transparent white-gray. The ADP is shown with ball-and-stick model. The important active site residues are depicted in licorice representation. The Mg^{2+} and Na^{+} ions are shown in green and yellow transparent balls, respectively. Water molecules coordinating Mg^{2+} ions are shown in transparent pink color. Some of the hydrogen bonds present are depicted with dashed bonds.

$\alpha = 0.42$, has the N6 amide of the adenine ring hydrogen-bonded with the side chain of D328 and the backbone carbonyl of D329. Hydrophobic stacking of the adenine ring with the underlying phenol ring of Y330 further stabilizes this intermediate. Thus, the D328-D329-Y330 motif appears to provide an adenine anchorage site. In addition to this surface patch, ADP anchors PKA through associated Mg^{2+} ions. Specifically, Mg1 coordinates D184 carboxyl in a monodentate way, whereas Mg2 coordinates E170 in a bidentate way.

Unexpectedly, interactions between adenine and these residues are persistent in the presence of Mg^{2+} ions (Figure 6A), but deteriorate quickly in their absence (Figure 6B). This is reflected in the depth of the corresponding wells in the PMF (see Figures 2 and 3A,B). In the absence of Mg^{2+} ions, three Na^{+} ions form a highly labile complex with the phosphates to compensate their

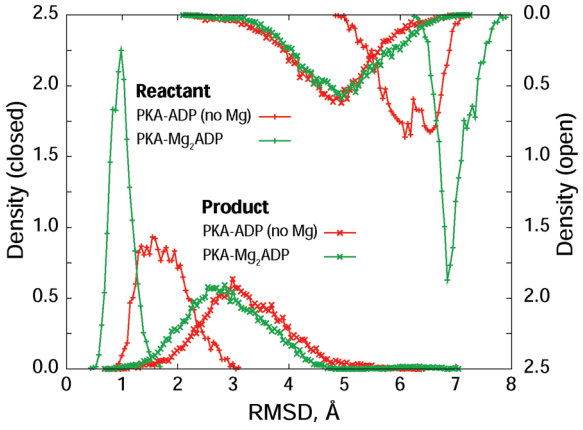

FIGURE 7: RMSD histograms for the Gly-rich loop residues 49 through 58 computed after aligning the structures for the product and reactant states defined in the text to the PDB structures representing closed (1L3R) and open (1J3H) states of PKA by the rigid core. The histograms with respect to closed state are shown using left and bottom axes, whereas the histograms with respect to open state are inverted and use right and top axes.

negative charge. Thus, the Mg^{2+} ions coordinated to the ADP appear to enhance interactions of the adenine with the anchoring residues D328, D329, and Y330.

Flexibility of the Gly-Rich Loop. Opening of the Gly-rich loop has been suggested to facilitate ADP release. Here we directly analyzed how the flexibility of the Gly-rich loop changes during nucleotide release. On the basis of PMF inspection, we define the reactant state as a combination of the beads 1 through 18 ($\alpha = 0.0$ to 0.09) and the product state as beads 113 through 185 ($\alpha = 0.61$ to 1.0).

With the Mg^{2+} ions coordinated to ADP in the reactant state, the Gly-rich loop is relatively rigid (as is seen from the RMSD histograms Figure 7 and analysis of dihedral angle distributions in residues 49 through 58 in Figure S1 of Supporting Information). Absence of Mg^{2+} ions in the active site renders the Gly-rich loop more flexible. This is revealed both by the corresponding RMSD histogram and an activation of a spontaneous peptide flip transition between T51 and G52 residues in the reactant state.

Upon ADP release, the Gly-rich loop motions enhance further, both internally (dihedral angles) and relative to the large lobe (RMSD). The dihedral angle analysis reveals that the peptide plane between T51 and G52 spontaneously flips back and forth during the unbinding process. Because Mg^{2+} ions do not affect the unbound product state (Figure 5A,B), Gly-rich loop fluctuations become similar in both paths. The final loop conformation in the product state appears intermediate between closed and open conformations defined by the crystal structures of 1L3R and 1J3H, respectively.

A good correlation between the Gly-rich loop motion and relative positions of two important hydrophobic residues, namely, Phe54 and Phe187, is observed. These residues help shield the active site from water in the closed state. In the reactant, with the nucleotide and two Mg^{2+} ions bound, their conformations are similar to those in the crystal structure with PDB code 1L3R. When we remove the two Mg^{2+} ions, both Phe54 and Phe187 move substantially from their original positions in the crystal structure and from each other. In the product state, once the nucleotide is out of the pocket, Phe54 moves by about 5−6 Å from Phe187, which settles back near its original

position. Thus, it appears that Mg^{2+} ions help to shield the active site from water even in the absence of the substrate.

Flexibility of the DFG Motif. Throughout the ADP release, PKA remained in its active state, showing no significant conformational changes in the DFG motif. Therefore, DFG flip is a rare event. To study the effect of DFG-flip on the ADP release, it would be necessary to enforce it artificially.

DISCUSSION

Here, we have computed a transition path ensemble for ADP release from PKA in the presence of two Mg^{2+} ions. Along this path we have calculated free energies required to release ADP in both the presence and absence of Mg^{2+}. To better understand the ADP release mechanism, we have dissected the PMFs into individual contributions from important functional groups. Specifically, we have examined contributions from each Mg^{2+} ion (Mg1 and Mg2), as well as the adenine, ribose, and pyrophosphate groups of ADP. We have also analyzed the conformational rearrangements and flexibilities of active site residues and of the Gly-rich loop.

ADP Release PMFs and Their Decompositions. Our PMFs demonstrate the strong binding free energy of ADP to PKA (−108.1 (−97.3) kcal/mol) in the presence of Mg^{2+} ions. Removal of both Mg^{2+} ions greatly reduces ADP binding free energy (to −22.0 (−11.2) kcal/mol) and introduces a significant association barrier that is not evident in the presence of Mg^{2+}. Experimentally, binding of nucleotides to PKA at high Mg^{2+} concentrations has been demonstrated to be diffusion controlled (*35*). This result is consistent with our calculations. The computed PMFs suggest that PKA must undergo some major structural change, such as local unfolding (*87*), to release ADP with Mg^{2+} ions. Otherwise, ADP can only dissociate from PKA following dissociation of the Mg^{2+} ions. Thus, Mg^{2+} appears to act as a linchpin in the rate-limiting ADP release.

A number of studies have addressed the driving forces underlying nucleotide association and the origins of cooperativity with Mg^{2+} ions (*23*, *32*, *46*). Of particular note was the thermodynamic characterization of ligand binding and its effect on thermostability of PKA for a series of ligands derived from ATP (*23*). Specifically, the series of ligands was designed by truncation of ATP to ADP, AMP (adenosine monophosphate), adenosine, and adenine. Thus, binding of both adenine and adenosine enhanced the stability of the C-subunit and required no Mg^{2+} ions. However, presence of the negatively charged phosphates destabilized nucleotide association and required Mg^{2+} ion presence to restore binding affinity. Two ions were necessary to achieve stabilizing effects comparable to the adenosine alone. Therefore, ion binding was beneficial only in the presence of the charged phosphate groups. Such "dissection" of binding into contributions from different groups suggested that the adenine moiety contributed to binding of nucleotide independently of Mg^{2+} ions. These findings correlated well with available thermodynamic measurements of binding constants for the ligands studied. Although highly successful in advancing our understanding of nucleotide binding and the origin of its cooperativity with Mg^{2+} ions, these studies lacked structural details and could not provide the precise contributions of individual groups to binding of a given nucleotide.

Adenine Independence of Mg^{2+}. PMF decomposition provides additional information regarding the mechanism of ADP binding. Specifically, our analysis indicates that the adenine group contribution is independent of Mg^{2+} presence. This is in agreement with the experimental results mentioned above (*23*, *88*). Therefore, the adenine group provides a constant driving force for nucleotide binding. The independence of the adenine binding from Mg^{2+} ions, allows us to predict that binding of ADP without Mg^{2+} ions would be 11.1 kcal/mol less favorable than that of the adenine alone.

In contrast to adenine, the ribose and the pyrophosphate group contributions are greatly perturbed by Mg^{2+} ions. The contribution of the pyrophosphate group changes from favorable to strongly unfavorable upon removal of Mg^{2+}. The ribose contribution becomes more favorable, but insufficient to compensate that of pyrophosphate. Therefore, the negatively charged pyrophosphate drives the ADP release. The experimental observation that adenine or adenosine binding to the catalytic subunit of PKA is not noticeably affected by the presence of Mg^{2+} ions supports our results and further implicates the pyrophosphate group in binding cooperativity (*23*, *32*).

Binding Cooperativity. The effect of the Mg^{2+} ions on the binding of ADP is highly nonlinear. Specifically, the difference between ADP association free energies in the presence and absence of Mg^{2+} ions is −86.1 kcal/mol, whereas the overall direct contribution of the Mg^{2+} ions found by energy decomposition is only −33.3 kcal/mol (Table 1). Therefore, the association of ADP with the Mg^{2+} ions produces a much larger binding free energy than the sum of the two groups considered separately. This finding is consistent with the fact that binding of the ADP and Mg^{2+} ions to PKA is cooperative (*34*).

Interestingly, as seen from Table 1, the change in the free energy contribution of the pyrophosphate group upon association with the Mg^{2+} ions (−83.6 kcal/mol) is close to the overall binding free energy change of ADP due to association with ions (−86.0 kcal/mol). These observations suggest that the origin of the cooperativity lies in quenching of the negative charge on the pyrophosphate group that otherwise contributes unfavorably to the binding process.

Overall, the results of the current free energy calculations and their decomposition are in remarkable agreement with earlier experimental work that dissected "the nucleotide and metal-phosphate binding sites" (*23*, *32*, *46*).

Structural Changes Associated with ADP Release. In addition to free energy decomposition, our simulations provide structural details on the mechanism of ADP release and intricate details of cooperative interactions among ADP, Mg^{2+} ions, and PKA. Combining knowledge of structural changes with their corresponding free energy information provides a powerful tool for gaining mechanistic insight.

Key Structural Elements. Our simulations capture all the interactions that have been previously described crystallographically for adenine ring anchoring (*24*). For example, adenine insertion completes the so-called C-spine structure of PKA that couples the N- and C-terminal lobes (*60*). As these are well-established and do not depend on Mg^{2+} ions, we omit them from the further discussion. Below we concentrate on residues to which we can attribute a novel Mg^{2+}-dependent functional role.

The conserved D184-K72-E91 triad appears to serve multiple functions. Besides positioning the pyrophosphate group of the nucleotide in the presence of Mg^{2+} ions, it also encourages its release in their absence. Interestingly, our results suggest that N171 also plays a multifunctional role. On one hand, it helps coordinate Mg2 with its carbonyl, while anchored to the backbone of the catalytic loop D166 with its amide. On the other

hand, when Mg^{2+} ions are removed, the amide N171 coordinates the α-phosphate of the nucleotide and its carbonyl contacts either the 3′-OH of the nucleotide or the side chain of K168.

Yet another multifunctional cluster, K168-D166-T201, performs different Mg^{2+}-dependent roles. K168 is known to bind γ-phosphate of ATP during catalysis (*27*−*31*). In our study, in the absence of Mg^{2+} ions, K168 binds the α- and β-phosphates of the nucleotide. In the presence of Mg^{2+} ions, K168 resides outside the active site and is able to pull up the side chain of E170. Although E170 has not been observed in the upward lifted conformation in PKA, there are precedents in a related kinase PDK1 (*89*). The D166 is known to coordinate the substrate OH group during phosphorylation and is able to reach water molecules in the first coordination shell of the Mg^{2+} ions. Yet in the absence of the substrate and Mg^{2+} ions this residue moves away from the active site to establish contact with the conserved T201 residue from peptide positioning loop.

Effect of Mg^{2+} Ions on the ADP Release Mechanism. The ADP release mechanism suggested by the optimized path in the presence of Mg^{2+} ions has the adenine group swing out of its binding pocket first, followed by the ribose and, finally, dissociation of the pyrophosphate group. Interestingly, a very similar sequence of events was observed in simulations where ADP was pulled from the binding pocket using SMD simulations in the absence of Mg^{2+} ions (*51*). The agreement between the two independent simulations is particularly good during the early stages of nucleotide release. However, the paths diverge once the adenine group has left its binding pocket.

Although we have not optimized the ADP release path in the absence of Mg^{2+} ions, we refer to the free energy decomposition to gain additional insights into the effect of Mg^{2+} ions on the dissociation mechanism. Because the negatively charged pyrophosphate of ADP provides significant impetus for ADP dissociation, it would seem that pyrophosphate would not act as an anchor in the absence of Mg^{2+} ions. Our simulations suggest that with the Mg^{2+} ions removed, the pyrophosphate is coordinated by K72, K168, and N171 residues and in addition by the nest on the Gly-rich loop. However, even combined these interactions are not strong enough to combat the repulsive drive from the negatively charged residues in the vicinity, particularly E127, D184, E170, and D166. Note that strong repulsive electrostatic interactions between the pyrophosphate and D184 as well as other neighboring anionic residues have been suggested previously as the driving force for ADP release (*47*). Thus, based on the free energy decomposition, it appears that the pyrophosphate can dissociate from PKA in the absence of Mg^{2+} ions at any time. This proposal is different from the SMD-derived mechanism, but is consistent with the fact that in crystal structures of bound nucleotide at low Mg^{2+} concentrations the positions of the β- and γ-phosphates are often disordered (*20*, *24*).

Three Cation-Binding Sites Created by Nucleotide Binding. Our simulations demonstrate that ADP binding creates three cation-binding sites at the ADP/PKA interface that are absent in nucleotide free PKA (see Supporting Information for details). Two of these sites employ the pyrophosphate group of the nucleotide, along with active site residues, to coordinate the linchpin Mg^{2+} ions. The third site utilizes the ribose hydroxyl groups and residues E127 and Y330. We note that this previously unreported site utilizes the same residues that coordinate an invariant P-3 Arg residue from substrate and inhibitor peptides (*24*). Formation of this nucleotide-dependent cation-binding site may therefore operate as a functionally important sensor for the closed C-subunit. We postulate that this binding site may be linked to the absolute requirement for Mg^{2+}-nucleotide binding prior to complex formation with RI inhibitor or PKI (*8*, *43*, *90*−*92*), and furthermore determine the specific order of the underlying binding events (*8*, *9*, *47*, *91*, *93*).

Inhibitory versus Activating Mg^{2+} Binding Site. Mg^{2+} binding has been previously probed with various physicochemical techniques (*24*, *32*, *34*, *35*, *46*). It was demonstrated that the two major binding sites are not coupled. That is binding at one site can be considered independent of the occupancy of the other site. These studies have also indicated that activating site (Mg1) has higher affinity for Mg^{2+} than the inhibitory site (Mg2) (*24*, *34*, *35*). The inhibitory Mg2 has been shown to affect the rate of catalysis by inhibiting ADP release (*33*, *45*, *94*, *95*). However, a detailed mechanism of this inhibition has not yet been established.

Recall that with ATP, Mg1 binds β- and γ-phosphates, whereas Mg2 binds α- and γ-phosphates (*34*). The γ-phosphate transfer causes the coordination shells of both ions to rearrange such that Mg1 now binds only β-phosphate, whereas Mg2 binds α- and β-phosphate (assuming phosphorylated product has dissociated from PKA leaving Mg^{2+} behind). This in turn causes the binding constants of the two Mg^{2+} ions to become equal as determined experimentally. Surprisingly, our free energy decomposition demonstrates that Mg2 contributes to binding of ADP almost twice as much as Mg1, reminiscent of its contribution to stabilizing of the transition state in the phosphoryl transfer reaction predicted by QM/MM (*31*). These contributions, however, are different from the experimentally measured binding free energies, and are the opposite of those expected for ATP. The QM/MM calculations that predict phosphoryl transfer rate enhancement due to Mg2 also differ from the kinetic studies that have indicated that the transfer rate is independent of the second Mg^{2+} ion (*23*, *37*). Thus the experimental and computational studies appear to create a controversy regarding the individual roles of Mg^{2+} ions.

The change in Mg^{2+} binding affinity upon γ-phosphate transfer (followed by product release) predicted by the present study could rationalize how the weakly ATP-bound Mg2 inhibits PKA catalysis. Specifically, upon γ-phosphate transfer from ATP the weakly bound Mg2 ion would become strongly bound, and would therefore inhibit the release of ADP. This proposal is consistent with the prevalent binding mode of Mg^{2+} to ADP in solution (*34*, *35*, *96*).

On-Path Intermediate. Analyzing the PMF for ADP unbinding with Mg^{2+} ions highlighted a metastable intermediate (Figure 6). Corresponding structural analysis identified hydrogen-bonding interactions from the side chain of D328 and backbone of D329 to the N6 amide of ADP along with hydrophobic interactions from Y330. Besides these interactions, ADP was anchored to E170 and D184 carboxyl oxygens through associated Mg^{2+} ions. Such an intermediate was not apparent in a previous steered MD study performed in the absence of Mg^{2+} ions (*51*). The free energy profiles (Figure 2) have confirmed absence of this intermediate upon removal of the Mg^{2+} ions. This metastable intermediate underscores the important role of the E170 residue, which would be difficult to identify experimentally.

Even though structural analysis clearly identified two sets of interactions of ADP with PKA in the intermediate, one set turns out to be relatively unimportant energetically. Specifically, free energy decomposition (Figure 3) shows that the intermediate is predominantly due to the pyrophosphate group of ADP along

with Mg^{2+} ions and not due to the adenine ring. Therefore, the adenine anchoring at the surface patch of residues D328, D329, and Y330 is in fact inconsequential in the absence of Mg^{2+} ions.

Residues D328, D329, and Y330 from the anchoring patch are part of a larger D328DYEEEE patch that has been shown to be sensitive to conformational changes, and in particular to ATP and inhibitor binding (*24*). The same patch has been identified through fragment binding assays as important for allosteric regulation of PKA (*97*). Recall that residue Y330 along with E127 and the 2′-OH group of ADP forms the high affinity cation-binding site that binds absolutely conserved P-3 arginine of substrate or inhibitor peptides.

Main Chain Conformational Changes. The Gly-rich loop pins down the nucleotide's phosphates helping to ensure the proper positioning of the γ-phosphate for phosphoryl transfer. It has been suggested that the small lobe that provides the Gly-rich loop can move with respect to the large lobe to open the active site cleft. In addition, the Gly-rich loop itself can move relative to the small lobe to modulate the opening of the active site cleft. To facilitate rate-limiting ADP release, the Gly-rich loop along with the small lobe have been proposed to assume an open conformation (*33*, *36*, *37*, *42*, *44*, *45*, *95*). Our simulations show the considerable opening of the Gly-rich loop during the ADP release and support this suggestion.

Furthermore, we have found that Mg^{2+} ions can modulate opening of the Gly-rich loop. Comparing simulations with and without Mg^{2+} ions in the active site, we find that the Gly-rich loop prefers a more closed conformation in the presence of Mg^{2+}. When the Mg^{2+} ions have been removed from the active site, the Gly-rich loop becomes more flexible as evidenced by its RMSD in Figure 7 and activation of the rotation for the peptide plane between residues T51 and G52 (shown in Supporting Information). Although we do not have direct evidence for Gly-rich loop motions facilitating ADP release, we note a correlation between the degree of flexibility of the loop and the bound Mg^{2+} ions. Thus higher flexibility of the loop corresponds to lower binding affinity and more facile release of ADP from PKA. This observation appears to be in good agreement with the X-ray data on the ADP ternary complex, where the Gly rich loop was observed to be somewhat flexible along with the β-phosphate of ADP (*20*).

The spontaneous rotations of the peptide plane between T51 and G52 can influence the dipolar balance in the loop that glues it to the phosphates and to the large lobe in the reactant state. Furthermore, rotation of the peptide bond can also serve as a gate for ADP release from under the Gly-rich loop that acts as a lid to the active site. Interestingly the G52 mutation has been found to be the most important for catalysis (*98*). However, only mutations at G50 affected binding of ADP directly, suggesting that the detected rotation is not essential for ADP release.

Finally, our simulations indicate that the DFG motif remains in the active conformation along the whole path of ADP release from the binary complex to the apoenzyme. In agreement, previous MD simulations on Abl kinase have suggested that the DFG flip is a rare event (*40*). Our study suggests further that the DFG flip is off path for the nucleotide release. We believe that the DFG flip in the closed state with ADP and Mg^{2+} ions bound would be strongly unfavorable due to the Mg^{2+} coordination of the DFG motif through the D184 residue. Therefore, similar to ADP release, the DFG flip would require prior Mg^{2+} dissociation.

CONCLUSIONS

Overall, we find simultaneous release of ADP with two Mg^{2+} ions from PKA to be so unfavorable that it would require local unfolding of the enzyme or some other major conformational change to disassemble the complex. On the other hand, removal of Mg^{2+} ions substantially accelerates release of ADP. Therefore, we conjecture that Mg^{2+} ions act as linchpins to ADP dissociation. Hence, a likely dissociation mechanism entails ADP release following Mg^{2+} ion dissociation.

Although the optimized path for the ADP release with Mg^{2+} ions resembles the path obtained without Mg^{2+} in previous SMD simulations, with the adenine ring leaving the binding site first (*51*), our free energy analysis suggests a different dissociation sequence. Specifically, in the absence of Mg^{2+} ions the pyrophosphate group provides strong impetus for nucleotide dissociation from PKA acting as a float. On the other hand, compensating for the charge on the pyrophosphate group by association with Mg^{2+} ions removes the dissociation driving force and is responsible for the binding cooperativity.

According to our calculations, Mg^{2+}-independent adenine binding drives the nucleotide association with PKA. This binding creates three cation-binding sites (see Figure 4A) at the protein−nucleotide interface that are otherwise absent. One of these sites coincides with the binding site for the conserved P-3 Arg from substrate and inhibitor peptides (see Figure 1). Appearance of this site may serve as a reporter of active site occupation and may explain cooperativity of binding between the nucleotide and PKA inhibitor or substrate proteins.

Finally, our study identifies several residues, namely, D166, K168, E170, N171, D184, and T201 that along with Gly-rich loop undergo specific conformational changes in response to binding or release of Mg^{2+} ions in the active site. The process of ADP binding with Mg^{2+} ions, involves a series of carboxylate shifts that begins with residue D184 and ends with E170 (see Supporting Information). These conserved residues, therefore, play important Mg^{2+}-dependent roles in nucleotide binding. Dissociation of Mg^{2+} ions makes Gly-rich loop more flexible in the ADP-bound state. In the product state, in which ADP has left the active site, the Gly-rich loop assumes the conformation that is intermediate between the open and closed states.

The results of this work further understanding of small ligand binding to proteins in general, and their role in the allosteric regulation of the PKA in particular. Thus, the study prepares grounds for future work on the allosteric mechanisms in the holoenzyme complex. Finally, insights from this study may contribute to developing new kinase drug design strategies.

ACKNOWLEDGMENT

The computations described in this paper were made possible by a generous teragrid MRAC awards (TG-MCB080040N and TG-MCA93T013) from NCSA on Abe supercomputer, and in-house computer cluster acquired through HHMI. The authors thank Professor J. Adams, Professor J. Weare, and Dr. Y. Cheng for helpful discussions, and especially Dr. A. Kornev for critical reading of the manuscript and suggested improvements.

SUPPORTING INFORMATION AVAILABLE

Details of model setup, transition path optimization, and PMF calculations along with protocols and results of analysis. Figure 1S A,B illustrates peptide bond conformation between residues

T51 and G52. The results and the protocol of Bio3D analysis of the structures of PKA available from PDB and from the simulated trajectories are also provided. Full author name for ref *63*. This material is available free of charge via the Internet at http://pubs.acs.org.

REFERENCES

1. Smith, C. M., Radzio-Andzelm, E., Madhusudan, Akamine, P., and Taylor, S. S. (1999) The catalytic subunit of cAMP-dependent protein kinase: prototype for an extended network of communication. *Prog. Biophys. Mol. Biol. 71*, 313–341.
2. Taylor, S. S., Radzio-Andzelm, E., Madhusudan, Cheng, X., Ten Eyck, L., and Narayana, N. (1999) Catalytic subunit of cyclic AMP-dependent protein kinase: structure and dynamics of the active site cleft. *Pharmacol. Ther. 82*, 133–141.
3. Johnson, D. A., Akamine, P., Radzio-Andzelm, E., Madhusudan, and Taylor, S. S. (2001) Dynamics of cAMP-dependent protein kinase. *Chem. Rev. 101*, 2243–2270.
4. Nolen, B., Taylor, S., and Ghosh, G. (2004) Regulation of protein kinases: Controlling activity through activation segment conformation. *Mol. Cell 15*, 661–675.
5. Taylor, S. S., Kim, C., Vigil, D., Haste, N. M., Yang, J., Wu, J., and Anand, G. S. (2005) Dynamics of signaling by PKA. *Biochim. Biophys. Acta 1754*, 25–37.
6. Manning, G., Whyte, D. B., Martinez, R., Hunter, T., and Sudarsanam, S. (2002) The protein kinase complement of the human genome. *Science 298*, 1912–1934.
7. Adams, J. A. (2001) Kinetic and catalytic mechanisms of protein kinases. *Chem. Rev. 101*, 2271–2290.
8. Herberg, F. W., and Taylor, S. S. (1993) Physiological inhibitors of the catalytic subunit of cAMP-dependent protein kinase: effect of MgATP on protein−protein interactions. *Biochemistry 32*, 14015–14022.
9. Zimmermann, B., Schweinsberg, S., Drewianka, S., and Herberg, F. W. (2008) Effect of metal ions on high-affinity binding of pseudosubstrate inhibitors to PKA. *Biochem. J. 413*, 93–101.
10. Herberg, F. W., Yonemoto, W., and Taylor, S. S. (1993) The catalytic subunit of cAMP-dependent protein kinase. *NATO ASI Ser., Ser. H 76*, 203–213.
11. Taylor, S. S., Knighton, D. R., Zheng, J., Ten Fyck, L. F., and Sowadski, J. M. (1992) Structural framework for the protein kinase family. *Annu. Rev. Cell Biol. 8*, 429–462.
12. Taylor, S. S., Knighton, D. R., Zheng, J., Ten Eyck, L. F., and Sowadski, J. M. (1992) cAMP-dependent protein kinase and the protein kinase family. *Faraday Discuss.* 143–152.
13. Zheng, J., Knighton, D. R., Nguyen, H. X., Taylor, S. S., Sowadski, J. M., and Ten Eyck, L. F. (1993) Crystal structures of the myristylated catalytic subunit of cAMP-dependent protein kinase reveal open and closed conformations. *Protein Sci. 2*, 1559–1573.
14. Narayana, N., Cox, S., Nguyen-huu, X., Ten Eyck, L. F., and Taylor, S. S. (1997) A binary complex of the catalytic subunit of cAMP-dependent protein kinase and adenosine further defines conformational flexibility. *Structure 5*, 921–935.
15. Tsigelny, I., Greenberg, J. P., Cox, S., Nichols, W. L., Taylor, S. S., and Ten Eyck, L. F. (1999) 600 ps molecular dynamics reveals stable substructures and flexible hinge points in cAMP dependent protein kinase. *Biopolymers 50*, 513–524.
16. Helms, V., and McCammon, J. A. (1997) Kinase conformations: a computational study of the effect of ligand binding. *Protein Sci. 6*, 2336–2343.
17. Cheng, X., Shaltiel, S., and Taylor, S. S. (1998) Mapping substrate-induced conformational changes in cAMP-dependent protein kinase by protein footprinting. *Biochemistry 37*, 14005–14013.
18. Watson, J. D., and Milner-White, E. J. (2002) A novel main-chain anion-binding site in proteins: the nest. A particular combination of [phi],[psi] values in successive residues gives rise to anion-binding sites that occur commonly and are found often at functionally important regions. *J. Mol. Biol. 315*, 171–182.
19. Watson, J. D., and Milner-White, E. J. (2002) The conformations of polypeptide chains where the main-chain parts of successive residues are enantiomeric. Their occurrence in cation and anion-binding regions of proteins. *J. Mol. Biol. 315*, 183–191.
20. Madhusudan, Trafny, E. A., Nguyen Huu, X., Adams, J. A., Ten Eyck, L. F., Taylor, S. S., and Sowadski, J. M. (1994) cAMP-dependent protein kinase: crystallographic insights into substrate recognition and phosphotransfer. *Protein Sci. 3*, 176–187.
21. Karlsson, R., Madhusudan, Taylor, S. S., and Sowadski, J. M. (1994) Intermolecular contacts in various crystal forms related to the open and closed conformational states of the catalytic subunit of cAMP-dependent protein kinase. *Acta Crystallogr., Sect D: Biol. Crystallogr. D50*, 657–662.
22. Akamine, P., Madhusudan, Wu, J., Xuong, N.-H., Ten Eyck, L. F., and Taylor, S. S. (2003) Dynamic features of cAMP-dependent protein kinase revealed by apoenzyme crystal structure. *J. Mol. Biol. 327*, 159–171.
23. Herberg, F. W., Doyle, M. L., Cox, S., and Taylor, S. S. (1999) Dissection of the nucleotide and metal-phosphate binding sites in cAMP-dependent protein kinase. *Biochemistry 38*, 6352–6360.
24. Zheng, J., Knighton, D. R., Ten Eyck, L. F., Karlsson, R., Xuong, N. H., Taylor, S. S., and Sowadski, J. M. (1993) Crystal structure of the catalytic subunit of cAMP-dependent protein kinase complexed with MgATP and peptide inhibitor. *Biochemistry 32*, 2154–2161.
25. Yang, J., Ten Eyck, L. F., Xuong, N.-H., and Taylor, S. S. (2004) Crystal structure of a cAMP-dependent protein kinase mutant at 1.26 Å: New insights into the catalytic mechanism. *J. Mol. Biol. 336*, 473–487.
26. Shaltiel, S., Cox, S., and Taylor, S. S. (1998) Conserved water molecules contribute to the extensive network of interactions at the active site of protein kinase A. *Proc. Natl. Acad. Sci. U.S.A. 95*, 484–491.
27. Valiev, M., Kawai, R., Adams, J. A., and Weare, J. H. (2003) The role of the putative catalytic base in the phosphoryl transfer reaction in a protein kinase: First-principles calculations. *J. Am. Chem. Soc. 125*, 9926–9927.
28. Valiev, M., Yang, J., Adams, J. A., Taylor, S. S., and Weare, J. H. (2007) Phosphorylation reaction in cAPK protein kinase-free energy quantum mechanical/molecular mechanics simulations. *J. Phys. Chem. B 111*, 13455–13464.
29. Diaz, N., and Field, M. J. (2004) Insights into the phosphoryl-transfer mechanism of cAMP-dependent protein kinase from quantum chemical calculations and molecular dynamics simulations. *J. Am. Chem. Soc. 126*, 529–542.
30. Henkelman, G., LaBute, M. X., Tung, C.-S., Fenimore, P. W., and McMahon, B. H. (2005) Conformational dependence of a protein kinase phosphate transfer reaction. *Proc. Natl. Acad. Sci. U.S.A. 102*, 15347–15351.
31. Cheng, Y., Zhang, Y., and McCammon, J. A. (2005) How does the cAMP-dependent protein kinase catalyze the phosphorylation reaction: An ab initio QM/MM study. *J. Am. Chem. Soc. 127*, 1553–1562.
32. Cook, P. F., Neville, M. E. Jr., Vrana, K. E., Hartl, T. F., and Roskoski, R. Jr. (1982) Adenosine cyclic 3′,5′-monophosphate dependent protein kinase: Kinetic mechanism for the bovine skeletal muscle catalytic subunit. *Biochemistry 21*, 5794–5799.
33. Shaffer, J., and Adams, J. A. (1999) An ATP-linked structural change in protein kinase A precedes phosphoryl transfer under physiological magnesium concentrations. *Biochemistry 38*, 5572–5581.
34. Armstrong, R. N., Kondo, H., Granot, J., Kaiser, E. T., and Mildvan, A. S. (1979) Magnetic resonance and kinetic studies of the manganese(II) ion and substrate complexes of the catalytic subunit of adenosine 3′,5′-monophosphate dependent protein kinase from bovine heart. *Biochemistry 18*, 1230–1238.
35. Granot, J., Mildvan, A. S., and Kaiser, E. T. (1980) Studies of the mechanism of action and regulation of cAMP-dependent protein kinase. *Arch. Biochem. Biophys. 205*, 1–17.
36. Adams, J. A., and Taylor, S. S. (1993) Divalent metal ions influence catalysis and active-site accessibility in the cAMP-dependent protein kinase. *Protein Sci. 2*, 2177–2186.
37. Shaffer, J., and Adams, J. A. (1999) Detection of conformational changes along the kinetic pathway of protein kinase A using a catalytic trapping technique. *Biochemistry 38*, 12072–12079.
38. Kornev, A. P., Haste, N. M., Taylor, S. S., and Eyck, L. F. (2006) Surface comparison of active and inactive protein kinases identifies a conserved activation mechanism. *Proc. Natl. Acad. Sci. U.S.A. 103*, 17783–17788.
39. Kannan, N., and Neuwald, A. F. (2005) Did protein kinase regulatory mechanism evolve through elaboration of a simple structural component? *J. Mol. Biol. 351*, 956–972.
40. Shan, Y., Seeliger, M. A., Eastwood, M. P., Frank, F., Xu, H., Jensen, M. O., Dror, R. O., Kuriyan, J., and Shaw, D. E. (2009) A conserved protonation-dependent switch controls drug binding in the Abl kinase. *Proc. Natl. Acad. Sci. U.S.A. 106*, 139–144.
41. Adams, J. A., and Taylor, S. S. (1992) Energetic limits of phosphotransfer in the catalytic subunits of cAMP-dependent protein kinase as measured by viscosity experiments. *Biochemistry 31*, 8516–8522.

42. Ni, D. Q., Shaffer, J., and Adams, J. A. (2000) Insights into nucleotide binding in protein kinase A using fluorescent adenosine derivatives. *Protein Sci. 9*, 1818–1827.
43. Neitzel, J. J., Dostmann, W. R. G., and Taylor, S. S. (1991) Role of magnesium-ATP in the activation and reassociation of cAMP-dependent protein kinase I: consequences of replacing the essential arginine in cAMP-binding site A. *Biochemistry 30*, 733–739.
44. Lew, J., Taylor, S. S., and Adams, J. A. (1997) Identification of a partially rate-determining step in the catalytic mechanism of cAMP-dependent protein kinase: A transient kinetic study using stopped-flow fluorescence spectroscopy. *Biochemistry 36*, 6717–6724.
45. Zhou, J., and Adams, J. A. (1997) Participation of ADP dissociation in the rate-determining step in cAMP-dependent protein kinase. *Biochemistry 36*, 15733–15738.
46. Bhatnagar, D., Roskoski, R., Rosendahl, M. S., and Leonard, N. J. (1983) Adenosine cyclic 3′,5′-monophosphate dependent protein kinase: a new fluorescence displacement titration technique for characterizing the nucleotide binding site on the catalytic subunit. *Biochemistry 22*, 6310–6317.
47. Qamar, R., Yoon, M.-Y., and Cook, P. F. (1992) Kinetic mechanism of the adenosine 3′,5′-monophosphate dependent protein kinase catalytic subunit in the direction of magnesium adenosine 5′-diphosphate phosphorylation. *Biochemistry 31*, 9986–9992.
48. Isralewitz, B., Baudry, J., Gullingsrud, J., Kosztin, D., and Schulten, K. (2001) Steered molecular dynamics investigations of protein function. *J. Mol. Graphics Modell. 19*, 13–25.
49. Leech, J., Prins, J. F., and Hermans, J. (1996) SMD: visual steering of molecular dynamics for protein design. *IEEE Comput. Sci. Eng. 3*, 38–45.
50. Grubmueller, H., Heymann, B., and Tavan, P. (1996) Ligand binding: molecular mechanics calculation of the streptavidin-biotin rupture force. *Science 271*, 997–999.
51. Lu, B., Wong, C. F., and McCammon, J. A. (2005) Release of ADP from the catalytic subunit of protein kinase A: A molecular dynamics simulation study. *Protein Sci. 14*, 159–168.
52. Klahn, M., Rosta, E., and Warshel, A. (2006) On the mechanism of hydrolysis of phosphate monoesters dianions in solutions and proteins. *J. Am. Chem. Soc. 128*, 15310–15323.
53. Warshel, A., Sharma, P. K., Kato, M., Xiang, Y., Liu, H., and Olsson, M. H. M. (2006) Electrostatic basis for enzyme catalysis. *Chem. Rev. 106*, 3210–3235.
54. Khavrutskii, I. V., Gorfe, A. A., Lu, B., and McCammon, J. A. (2009) Free energy for the permeation of Na^+ and Cl^- ions and their ion-pair through zwitterionic dimyristoyl phosphatidylcholine lipid bilayer by umbrella integration with harmonic fourier beads. *J. Am. Chem. Soc. 131*, 1706–1716.
55. Khavrutskii, I. V., Fajer, M., and McCammon, J. A. (2008) Intrinsic free energy of the conformational transition of the KcsA signature peptide from conducting to nonconducting state. *J. Chem. Theor. Comp. 4*, 1541–1554.
56. Khavrutskii, I. V., Dzubiella, J., and McCammon, J. A. (2008) Computing accurate potentials of mean force in electrolyte solutions with the generalized gradient-augmented harmonic Fourier beads method. *J. Chem. Phys. 128* (044106), 1–13.
57. Khavrutskii, I. V., and McCammon, J. A. (2007) Generalized gradient-augmented harmonic Fourier beads method with multiple atomic and/or center-of-mass positional restraints. *J. Chem. Phys. 127* (124901), 1–12.
58. Khavrutskii, I. V., Arora, K., and Brooks, C. L. III (2006) Harmonic fourier beads method for studying rare events on rugged energy surfaces. *J. Chem. Phys. 125* (174108), 1–7.
59. Grant, B. J., Rodrigues, A. P., ElSawy, K. M., McCammon, J. A., and Caves, L. S. (2006) Bio3d: an R package for the comparative analysis of protein structures. *Bioinformatics 22*, 2695–2696.
60. Kornev, A. P., Taylor, S. S., and Ten Eyck, L. F. (2008) A helix scaffold for the assembly of active protein kinases. *Proc. Natl. Acad. Sci. U.S.A. 105*, 14377–14382.
61. MacKerell, A. D., Jr., Brooks, B. R., Brooks, C. L., III, Nilsson, L., Roux, B., Won, Y., Karplus, M. (1998) CHARMM: The energy function and its parameterization with an overview of the program, in The Encyclopedia of Computational Chemistry (Schleyer, P. v. R., Schreiner, P. R., Allinger, N. L., Clark, T., Gasteiger, J., Kollman, P., Henry F. Schaefer, I., Eds.) John Wiley & Sons, Chichester.
62. Phillips, J. C., Braun, R., Wang, W., Gumbart, J., Tajkhorshid, E., Villa, E., Chipot, C., Skeel, R. D., Kale, L., and Schulten, K. (2005) Scalable molecular dynamics with NAMD. *J. Comput. Chem. 26*, 1781–1802.
63. MacKerell, A. D. Jr.; et al. (1998) All-atom empirical potential for molecular modeling and dynamics Studies of proteins. *J. Phys. Chem. B 102*, 3586–3616.
64. MacKerell, A. D. Jr., Wiorkiewicz-Kuczera, J., and Karplus, M. (1995) An all-atom empirical energy function for the simulation of nucleic acids. *J. Am. Chem. Soc. 117*, 11946–11975.
65. Glenn, J. M., Douglas, J. T., and Michael, L. K. (1994) Constant pressure molecular dynamics algorithms. *J. Chem. Phys. 101*, 4177–4189.
66. Scott, E. F., Yuhong, Z., Richard, W. P., and Bernard, R. B. (1995) Constant pressure molecular dynamics simulation: The Langevin piston method. *J. Chem. Phys. 103*, 4613–4621.
67. Essmann, U., Perera, L., Berkowitz, M. L., Darden, T., Lee, H., and Pedersen, L. G. (1995) A smooth particle mesh Ewald method. *J. Chem. Phys. 103*, 8577–8593.
68. Darden, T., York, D., and Pedersen, L. G. (1993) Particle mesh Ewald: An N*log(N) method for Ewald sums in large systems. *J. Chem. Phys. 98*, 10089–10092.
69. Grubmueller, H., Heller, H., Windemuth, A., and Schulten, K. (1991) Generalized Verlet algorithm for efficient molecular dynamics simulations with long-range interactions. *Mol. Simulation 6*, 121–142.
70. Streett, W. B., Tildesley, D. J., and Saville, G. (1978) Multiple time-step methods in molecular dynamics. *Mol. Phys. 35*, 639–648.
71. Ryckaert, J.-P., Ciccotti, G., and Berendsen, H. J. C. (1977) Numerical integration of the cartesian equations of motion of a system with constraints: Molecular dynamics of *n*-alkanes. *J. Comp. Phys. 23*, 327–341.
72. Tobias, D. J., and Brooks, C. L. III (1988) Molecular dynamics with internal coordinate constraints. *J. Chem. Phys. 89*, 5115–5127.
73. Lazaridis, T., Tobias, D. J., Brooks, C. L. III, and Paulaitis, M. E. (1991) Reaction paths and free energy profiles for conformational transitions: an internal coordinate approach. *J. Chem. Phys. 95*, 7612–7625.
74. Roux, B., Nina, M., Pomes, R., and Smith, J. C. (1996) Thermodynamic stability of water molecules in the bacteriorhodopsin proton channel: A molecular dynamics free energy perturbation study. *Biophys. J. 71*, 670–681.
75. Gilson, M. K., Given, J. A., Bush, B. L., and McCammon, J. A. (1997) The statistical-thermodynamic basis for computation of binding affinities: A critical review. *Biophys. J. 72*, 1047–1069.
76. Hermans, J., and Wang, L. (1997) Inclusion of loss of translational and rotational freedom in theoretical estimates of free energies of binding. Application to a complex of benzene and mutant T4 lysozyme. *J. Am. Chem. Soc. 119*, 2707–2714.
77. Boresch, S., Tettinger, F., Leitgeb, M., and Karplus, M. (2003) Absolute binding free energies: A quantitative approach for their calculation. *J. Phys. Chem. A 107*, 9535–9551.
78. Deng, Y., and Roux, B. (2006) Calculation of standard binding free energies: Aromatic molecules in the T4 Lysozyme L99A Mutant. *J. Chem. Theor. Comp. 2*, 1255–1273.
79. Doudou, S., Burton, N. A., and Henchman, R. H. (2009) Standard free energy of binding from a one-dimensional potential of mean force. *J. Chem. Theor. Comp. 5*, 909–918.
80. Zhou, H.-X., and Gilson, M. K. (2009) Theory of free energy and entropy in noncovalent binding. *Chem. Rev. 109*, 4092–4107.
81. Knighton, D. R., Zheng, J. H., Ten Eyck, L. F., Xuong, N. H., Taylor, S. S., and Sowadski, J. M. (1991) Structure of a peptide inhibitor bound to the catalytic subunit of cyclic adenosine monophosphate-dependent protein kinase. *Science 253*, 414–420.
82. Gherman, B. F., Baik, M.-H., Lippard, S. J., and Friesner, R. A. (2004) Dioxygen activation in methane monooxygenase: A theoretical study. *J. Am. Chem. Soc. 126*, 2978–2990.
83. Torrent, M., Musaev, D. G., and Morokuma, K. (2001) The flexibility of carboxylate ligands in methane monooxygenase and ribonucleotide reductase: A density functional study. *J. Phys. Chem. B 105*, 322–327.
84. LeCloux, D. D., Barrios, A. M., Mizoguchi, T. J., and Lippard, S. J. (1998) Modeling the diiron centers of non-heme iron enzymes. Preparation of sterically hindered diiron(II) tetracarboxylate complexes and their reactions with dioxygen. *J. Am. Chem. Soc. 120*, 9001–9014.
85. Rardin, R. L., Tolman, W. B., and Lippard, S. J. (1991) Monodentate carboxylate complexes and the carboxylate shift: implications for polymetalloprotein structure and function. *New J. Chem. 15*, 417–430.
86. Sousa, S. F., Fernandes, P. A., and Ramos, M. J. (2007) The carboxylate shift in zinc enzymes: A computational study. *J. Am. Chem. Soc. 129*, 1378–1385.
87. Miyashita, O., Onuchic, J. N., and Wolynes, P. G. (2003) Nonlinear elasticity, proteinquakes, and the energy landscapes of functional transitions in proteins. *Proc. Natl. Acad. Sci. U.S.A. 100*, 12570–12575.

88. Sanders, C. R., Tian, G., and Tsai, M. D. (1989) Mechanism of adenylate kinase. Is there a relationship between local substrate dynamics, and local binding energy, and the catalytic mechanism? *Biochemistry 28*, 9028–9043.
89. Biondi, R. M., Komander, D., Thomas, C. C., Lizcano, J. M., Deak, M., Alessi, D. R., and van Aalten, D. M. F. (2002) High resolution crystal structure of the human PDK1 catalytic domain defines the regulatory phosphopeptide docking site. *EMBO J. 21*, 4219–4228.
90. Corbin, J. D., Keely, S. L., and Park, C. R. (1975) The distribution and dissociation of cyclic adenosine 3′:5′-monophosphate-dependent protein kinases in adipose, cardiac, and other tissues. *J. Biol. Chem. 250*, 218–225.
91. Whitehouse, S., and Walsh, D. A. (1983) Mg X ATP2-dependent interaction of the inhibitor protein of the cAMP-dependent protein kinase with the catalytic subunit. *J. Biol. Chem. 258*, 3682–3692.
92. Van Patten, S. M., Fletcher, W. H., and Walsh, D. A. (1986) The inhibitor protein of the cAMP-dependent protein kinase-catalytic subunit interaction. Parameters of complex formation. *J. Biol. Chem. 261*, 5514–5523.
93. Masterson, L. R., Mascioni, A., Traaseth, N. J., Taylor, S. S., and Veglia, G. (2008) Allosteric cooperativity in protein kinase A. *Proc. Natl. Acad. Sci. U.S.A. 105*, 506–511.
94. Zhou, J., and Adams, J. A. (1997) Is there a catalytic base in the active site of cAMP-dependent protein kinase? *Biochemistry 36*, 2977–2984.
95. Grant, B. D., and Adams, J. A. (1996) Pre-steady-state kinetic analysis of cAMP-dependent protein kinase using rapid quench flow techniques. *Biochemistry 35*, 2022–2029.
96. Huang, S. L., and Tsai, M. D. (1982) Does the magnesium(II) ion interact with the alpha-phosphate of ATP? An investigation by oxygen-17 nuclear magnetic resonance. *Biochemistry 21*, 951–959.
97. Yang, J., Kennedy, E. J., Wu, J., Deal, M. S., Pennypacker, J., Ghosh, G., and Taylor, S. S. (2009) Contribution of non-catalytic core residues to activity and regulation in protein kinase A. *J. Biol. Chem. 284*, 6241–6248.
98. Grant, B. D., Hemmer, W., Tsigelny, I., Adams, J. A., and Taylor, S. S. (1998) Kinetic analyses of mutations in the glycine-rich loop of cAMP-dependent protein kinase. *Biochemistry 37*, 7708–7715.